



Flow stability simulation over a stretching/shrinking surface with thermal radiation and viscous dissipation of hybrid nanofluids

S. V. Padma¹ · M. P. Mallesh¹ · M. Sanjalee² · Ali J. Chamkha³

Received: 28 October 2023 / Accepted: 16 December 2023 / Published online: 20 February 2024
© Akadémiai Kiadó, Budapest, Hungary 2024

Abstract

The main objective of this work is to investigate viscous dissipation with thermal radiation impact on hybrid nanofluid flow past an exponentially stretching/shrinking surface along with magnetic field, and heat source/sink, slip boundary conditions. Water (H_2O) is taken into account as a host fluid with copper (Cu) and alumina (Al_2O_3) as nanoparticles to form a hybrid nano liquid ($Cu-H_2O-Al_2O_3$). The coupled nonlinear partial differential equations are transmuted into ordinary differential equations using similarity transformations with boundary conditions and these ODEs are simplified using numerical solver, bvp4c in MATLAB. The behavior of momentum profiles, thermal profiles, coefficient of heat transfer (Nu_{x_1}) and skin friction (C_f) are explored using the pertinent parameters such as Eckert Number (Ec_1), Suction Parameter (S_1), Magnetic Parameter (M_1), Radiation Parameter (Nr_1), Stretching/Shrinking Parameter (λ), Velocity and thermal slip Parameters (A_1 and B_1), Heat source/sink Parameter (β_1), variable thermal Parameter (ϵ), thermal conductivity (K) are depicted through tables and graphs. The present simulation is more stable and convergence when compared with the existing literature, which is portrayed in the tables. The presence of dual solution is noticed for $Ec_1 = 0.1, 0.11, 0.12$ when the critical value of $\lambda (= \lambda_c)$ are $\lambda_{c_1} = -1.60355799, \lambda_{c_2} = -1.60322884$ and $\lambda_{c_3} = -1.6031348$, respectively. The existence of the dual solution is reported due to the presence of shrinking surface and suction, further, the first solution is found to be more stable. The novelty of the current simulation includes MHD hybrid nano liquid flow stability with the impact of viscous dissipation and thermal radiation past stretching/shrinking permeable plane to fill the research gap in the existing literature. The applications of transmission of heat by stretching/shrinking surface in boundary layers is used in various fields such as polymer and material processing, biomedical engineering, heat exchangers, etc.

Keywords Stretching/Shrinking sheet · bvp4c · Viscous dissipation · Thermal radiation · Slip conditions · Similarity Transformations

✉ M. P. Mallesh
malleshmardanpally@gmail.com
S. V. Padma
tumuluripadma@gmail.com
M. Sanjalee
maheshwari15sanjalee@gmail.com
Ali J. Chamkha
achamkha@yahoo.com

¹ Department of Mathematics, Koneru Lakshmaiah Education Foundation, Aziz Nagar, Hyderabad, Telangana 500075, India

² Department of Computer and Computational Sciences, Tribhuvan College of Environment and Development Sciences, Neemrana, Rajasthan 301705, India

³ Faculty of Engineering, Kuwait College of Science and Technology, 7th Ring Road, 35004 Doha District, Kuwait

List of Symbols

A_1	Momentum Slip Factor
B_1	Thermal Slip Factor
B_0	Magnetic Field Strength (Telsa (Ta))
C_p	Specific Heat ($J\ Kg^{-1}K^{-1}$)
$(\rho C_p)_{nf}$	Heat Capacitance of nanofluid ($JKg^{-1}K^{-1}$)
$(\rho C_p)_{hnf}$	HNF heat capacitance ($JKg^{-1}K^{-1}$)
Nu_{x_1}	Non-dimensional heat transfer coefficient
C_f	Coefficient of skin friction
L	Sheet length (m)
h_f	Coefficient of Convective Heat Transfer ($W/(m^2K)$)
Ec_1	Eckert number
M_1	Magnetic Parameter
Nr_1	Thermal Radiation Parameter
Pr_1	Prandtl number
q_r	Thermal Radiative Heat Flux (Wm^{-2})
q_w	Wall Heat Flux (Wm^{-2})

Re_{x_1}	Reynolds Number
S_1	Suction/Injection parameter
K	Thermal conductivity ($\text{Wm}^{-1}\text{K}^{-1}$)
T_1	Temperature (K)
T_{1_w}	Temperature at stretching/shrinking surface (K)
T_{1_∞}	Free Stream Temperature (K)
a_1, b_1	Constants
x_1, y_1	2D-space cartesian coordinates
u_1, v_1	Fluid velocity elements in x_1, y_1 -direction

Greek Letters

ϕ_1, ϕ_2	Nanoparticle volume fraction of Cu, Al_2O_3 respectively
η	Similarity variable
K	Thermal conductivity (Wm^{-1}K)
μ	Dynamic viscosity ($\text{Kg m}^{-1}\text{S}^{-1}$)
ν	Kinematic viscosity (m^2S^{-1})
ρ	Density (Kg m^{-3})
β_1	Heat Source/Sink Parameter
λ	Stretching/Shrinking parameter
σ	Electrical Conductivity (Ω/m)
σ^*	Stefan–Boltzmann Constant ($\text{W m}^{-2}\text{K}^{-4}$)
θ_1	Dimensionless temperature
ψ	Stream function
ϵ	Variable thermal conductivity parameter

Subscripts

f	Host fluid
nf	Nanofluid
hnf	Hybrid nanofluid

Introduction

The boundary layer behavior instigated by continuous stretching/shrinking plane plays an important role in manufacturing processes in Industries. The attributes of fluid motion over a stretching/shrinking porous plane with fluid viscosity as well as the cooling of permeable surface by polymer extrusion along stagnant fluid are a challenging problem in polymer industry. The hybrid nanofluid flow applications result more efficient in rate of heating/cooling enhancement.

Nanofluids have a great potential in improving thermal performance and the requirement of thermal efficacy is significant in the present micro-engineering content. Hence, the application of nanofluids is hugely expanding in several engineering industries, electrical and biomedicine. [1] first discussed the concept of nanofluid in 1995. The first research article on expandable surface in nanofluids which portrays the impacts of Brownian motion and thermophoresis using implicit finite difference method is introduced by [2]. [3] explained a numerical simulation on linear stretching surface of nano liquid flow with convective boundary conditions.

Brownian motion and thermophoresis effects on a non-linear stretching plane is numerically evaluated by [4]. [5] explored the hydromagnetic impact on nano liquid with gyrotactic microorganisms past a vertical expandable upright surface. Several researchers [6–10] investigated the applications of nano liquids on different geometries. Researcher [11] numerically examined the effect of magnetic field on the heat transfer rate of nanofluid in a square enclosure with wavy circular heater. [12] inspected the free convective heat transfer rate of nanofluid confined in square porous cavity saturated with nano-encapsulated phase change materials. As of late, [13] analyzed the thermal performance of non-Newtonian nano-encapsulated phase change materials in a slant channel with the complicated internal heat source.

Hybrid nanofluids are mixture of two or more different metals or non-metals with fundamental fluids like water, ethylene, engine oil unused which results more ability in heat transfer enhancement in contrast to nanofluids. Hybrid nanofluids with MHD have various applications in the fields of medicine, naval structures, solar energy conversion, defense, microelectronics, warming procedure in buildings, etc. Authors [14, 15] demonstrated the experimental analysis on hybrid nano liquid through heat exchangers. Other acceptable investigations on hybrid nano liquids are explored by the investigators [16–19]. [20] studied the magnetic radiative flow of hybrid nano liquid in three-dimensional flow with transmission of heat past a stretching sheet using Lobatto IIIA technique. The time-dependent Casson fluid flow with hybrid nano particles past a horizontal porous plane is numerically elaborated by [21]. [22] numerically examined the two-dimensional natural convective flow of hybrid nano liquid past an erect surface with magnetic and radiation. Numerical simulation of exponential shrinking surface of hybrid nano liquids with thermal energy is explored by [23]. Very recently the investigators [24–28] numerically evaluated the solutions on different geometries over stretching/shrinking surface. [29] numerically scrutinized unsteady hybrid nano liquid flow over an oscillating plate under heat generation and radiation effects.

In the analysis of a hybrid nanofluid boundary layer flow over stretching/shrinking surface, the terms heat generation/absorption, thermal radiation and viscous dissipation play a significant role in enhancement of heat transmission with magnetic effects. Several engineering applications are aerodynamics, paper production, geophysical flows, polymer processing flows, roofing materials, spinning of fibers, steam turbines, etc. Influence of thermal radiation over elongating/dwindling surface on convective flows are analyzed by several researchers [30–37]. [38] numerically examined the effect of radiation of nanofluid flow past an elongated plane with magnetism and viscous dissipation. A numerical simulation on nano liquid flow past an exponentially expandable

plane with influence of viscous-dissipation is studied by [39]. [40] theoretically and numerically investigated heat generation with thermophoresis on non-linear expandable sheet. Recently, the heat sink/source on steady state laminar flow of hybrid nano liquid along a nonlinear stretched plane with thermophoresis is numerically elaborated by [41]. Very recently, [42] studied about the numerical computation on hybrid CNTs past an exponentially elongated surface with slip flow with the influence of inclined Lorentz forces. The scrutinizer [43] monitored the effect of the periodic magnetic field on the free-convective heat transfer rate of alumina nano liquid in a hexagonal-enclosure. Several studies with suspension of nano-encapsulated phase change materials over different geometries is scrutinized by [44–46].

The inspiration behind the current article is aforementioned references in which several investigators presumed several fluids with distinct nanoparticles and a fascinating result for their thermal characteristics are observed. A novel scheme of two-dimensional stability simulation of MHD flow of hybrid nanofluid past an elongating/dwindling surface with impacts of radiation, slip boundary conditions and viscous dissipation is modelled in current numerical simulation. On employing similarity elements, the balanced equations of fluid flow equations (PDE's) in the transmuted into an ODE system. Numerical solver, namely bvp4c, utilizing MATLAB is employed to solve transmuted nonlinear coupled ODEs with boundary conditions. The graphical explanation is presented on velocity, temperature, coefficient of heat transfer and skin friction with varying parameters. An analysis of flow stability is found to stable and accuracy when compared with existing literature. The current work has novel characteristics that are helpful in many applications such as pharmaceutical processes, magnetic resonance imaging, dynamic sealing, thermal recovery of oil, etc.

Problem description

A system of cartesian coordinate with x_1 -coordinate normal to the y_1 -coordinate as portrayed in Fig 1., for an incompressible, laminar and steady, laminar flow of boundary layer of $Cu - Al_2O_3 - H_2O$ hybrid nano liquid toward an exponentially penetrable elongating/dwindling sheet in account of varied thermal conductivity and heat source/sink are considered. u_1, v_1 are the velocities in x_1, y_1 -directions, respectively. The surface velocity of stretching/shrinking sheet is represented as $u_{1w}(x_1) = c_1 e^{x_1/L}$. The heat source is $q = q_0 e^{x_1/L}$ and temperature as $T_1, T_{1w} = T_{1\infty} + T_{1_0} e^{x_1/2L}$ is the variable wall temperature with $T_{1_0} > 0$. $\lambda_1 > 0$ denotes the stretching surface whereas $\lambda_1 < 0$ and $\lambda_1 = 0$ denotes the expandable and motionless surface, respectively. $B_1 = B_0 e^{x_1/2L}$, an applied magnetic field with magnetic strength $-B_0$ is governed normal to the plane $y_1 = 0$. Tables 12 and 13 expose numerical values and heat transfer of fluids of two nanoparticles (Cu and Al_2O_3) with base fluid (H_2O). The below system of equations with aforementioned assumptions represents continuity, momentum and energy equations of fluid flow with boundary condition ([59]).

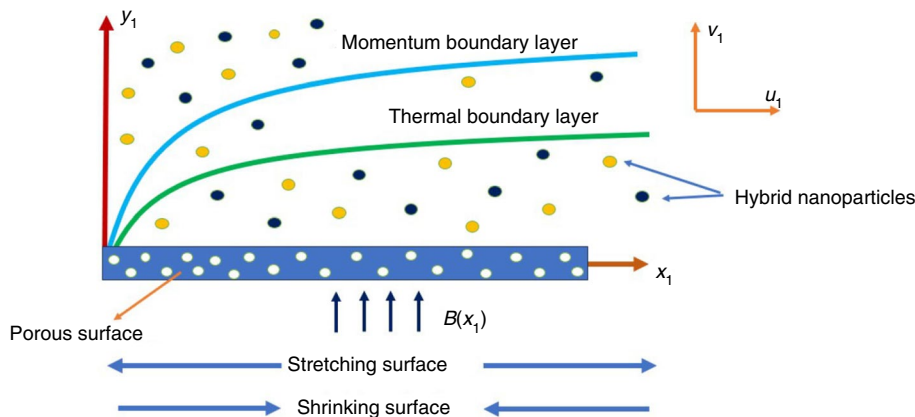
$$\frac{\partial u_1}{\partial x_1} + \frac{\partial v_1}{\partial y_1} = 0 \tag{1}$$

$$u_1 \frac{\partial u_1}{\partial x_1} + v_1 \frac{\partial u_1}{\partial y_1} = \frac{\mu_{hnf}}{\rho_{hnf}} \frac{\partial^2 u_1}{\partial y_1^2} - \frac{\sigma_{hnf}}{\rho_{hnf}} B^2 u_1 - \frac{\mu_{hnf}}{\rho_{hnf}} \frac{\epsilon}{k_1} \tag{2}$$

$$u_1 \frac{\partial T_1}{\partial x_1} + v_1 \frac{\partial T_1}{\partial y_1} = \frac{1}{(\rho C_p)_{hnf}} \frac{\partial}{\partial y_1} \left(K_{hnf}^* (T_1) \frac{\partial T_1}{\partial y_1} \right) - \frac{1}{(\rho C_p)_{hnf}} \frac{\partial q_r}{\partial y_1} - \frac{Q_1}{(\rho C_p)_{hnf}} (T_1 - T_{1\infty}) + \frac{\mu_{hnf}}{(\rho C_p)_{hnf}} \left(\frac{\partial u_1}{\partial y_1} \right)^2 \tag{3}$$

Boundary Conditions:

Fig. 1 Geometrical model



$$\begin{aligned}
 u_1 &= u_1(x_1)\lambda_1 + A_1 \frac{\mu_{\text{hnf}}}{\rho_{\text{hnf}}} \frac{\partial u_1}{\partial y_1}; v_1 = v_w; \\
 T_1 &= T_{1_w}(x) + B_1 \frac{\partial T_1}{\partial y_1} \text{ at } y_1 = 0, u_1 \rightarrow 0; \\
 T_1 &\rightarrow T_{1_\infty} \text{ at } y_1 \rightarrow \infty
 \end{aligned}
 \tag{4}$$

where $Q_1 = Q_0 e^{x_1/L}$ represents constant of heat source ([59]), $A_1 = a_1 e^{-x_1/2L}$ and $B_1 = b_1 e^{-x_1/2L}$ denotes the momentum and thermal slip factors dependent on x_1 (Yan et al.[43]). Heat capacitance $((\rho C_p)_{\text{hnf}})$, density (ρ_{hnf}) , dynamic viscosity (μ_{hnf}) , electric conductivity (σ_{hnf}) , thermal conductivity (K_{hnf}) , which are thermal physical attributes of fluid flow and active in Eqs (1)– (4) are explored in Table 11. Hybrid nano liquid have complex interactions among themselves and the fundamental fluid, which includes scattering, absorption and radiation. On considering this, Rosseland approximation [47] of thermal radiation for an optically dense layer, we have

$$q_r = -\frac{4\sigma^*}{3K^*} \frac{\partial T_1^4}{\partial y_1}, \tag{5}$$

here, σ^* is the constant of Stefan-Boltzmann, K = mean absorption coefficient. The term T_1^4 can be exposed a temperature linear function and expanding in Taylor series about T_{1_∞} and neglecting terms in higher order, we have

$$T_1^4 \cong 4T_{1_\infty}^3 T_1 - 3T_{1_\infty}^4. \tag{6}$$

The following represents the similarity transformations [48, 49] which gratify Eq. (1)

$$\begin{aligned}
 \psi &= e^{x_1/2L} \sqrt{2\nu_f L C_f} f_1(\eta); \eta = y e^{x_1/2L} \sqrt{\frac{c}{2\nu_f L}}; \\
 \theta_1 &= \frac{T_1 - T_{1_\infty}}{T_{1_w} - T_{1_\infty}}; u_1 = \frac{\partial \psi}{\partial y_1}; \\
 v_1 &= -\frac{\partial \psi}{\partial x_1}
 \end{aligned}
 \tag{7}$$

and reduce the aforementioned balanced Eq’s (2) - (4) as

$$\begin{aligned}
 \left(\frac{\mu_{\text{hnf}}/\mu_f}{\rho_{\text{hnf}}/\rho_f}\right) f_1'''' + 1 + f_1 f_1'' - 2f_1'^2 \\
 - \left(\frac{\sigma_{\text{hnf}}/\sigma_f}{\rho_{\text{hnf}}/\rho_f}\right) N_1 f_1' - \left(\frac{\mu_{\text{hnf}}/\mu_f}{\rho_{\text{hnf}}/\rho_f}\right) K f_1' = 0,
 \end{aligned}
 \tag{8}$$

$$\begin{aligned}
 \frac{1}{Pr_1} \left[\left(\frac{K_{\text{hnf}}}{K_f} (1 + \epsilon \theta_1) + Nr_1\right) \theta_1'' + \epsilon \frac{K_{\text{hnf}}}{K_f} \theta_1'^2 \right] \\
 + \left(\frac{(\rho C_p)_{\text{hnf}}}{(\rho C_p)_f}\right) (f_1 \theta_1' - f_1') \\
 + \beta_1 \theta_1 + \frac{\mu_{\text{hnf}}}{\mu_f} Ec_1 (f_1'')^2 = 0,
 \end{aligned}
 \tag{9}$$

where, the emerging parameters, Prandtl number = Pr_1 , Eckert number = Ec_1 , Magnetic field parameter = M_1 , Thermal radiation parameter = Nr_1 , Heat source/sink parameter = β , Wall mass transfer parameter = S_1 in which $S_1 > 0 (v_{1_0} < 0)$ = suction parameter and $S_1 < 0 (v_{1_0} > 0)$ = injection parameter and are defined as

$$\begin{aligned}
 Pr_1 &= \frac{\nu_f (\rho C_p)_f}{K_f}; Nr_1 = \frac{16\sigma^* T_{1_\infty}^3}{3K_f K^*}; \beta_1 = \frac{2Q_0 L}{c} (\rho C_p) f; \\
 Ec_1 &= \frac{(u_{1_w}(x))^2}{(T_{1_w} - T_{1_\infty})(C_p)_f}; M_1 = \frac{2B_0^2 L \sigma_f}{\rho_f c}; S_1 = -\frac{v_0}{\sqrt{\frac{\nu_f c}{2L}}}; \\
 K &= \frac{2L\nu_f}{K_1 u_w(x_1)}; u_{1_w}(x_1) = c e^{x_1 L},
 \end{aligned}
 \tag{10}$$

subjected to the boundary conditions

$$f_1 = S_1; f_1' = \lambda + A_1 f_1''; \theta_1 = 1 + B_1 \theta_1'; \text{ at } \eta = 0, \tag{11}$$

$$f_1' \rightarrow 0; \theta_1 \rightarrow 0 \text{ at } \eta \rightarrow \infty \tag{12}$$

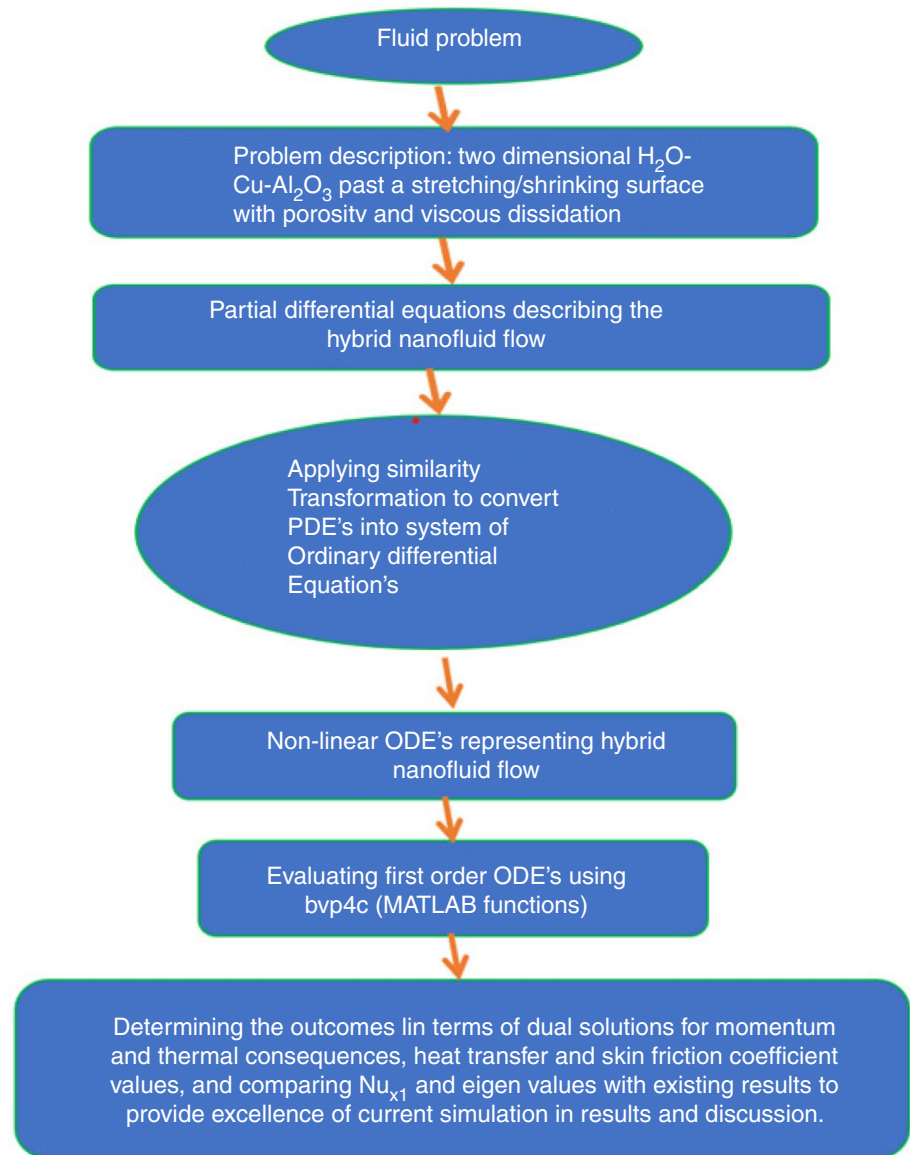
Here

$$A_1 = A_2 \frac{\mu_{\text{hnf}}}{\rho_{\text{hnf}}} \sqrt{\frac{c}{2\nu_f L}}; B_1 = B_2 \sqrt{\frac{c}{2\nu_f L}}. \tag{13}$$

Physical quantities

The physical quantities, important as to be worthy, like coefficient of skin friction, drag force and heat flux have ample applications such as skin friction coefficient is useful in understanding the resistance experienced by an object moving through a fluid, drag force is useful in designing vehicles, sports equipment and heat flux helps to design effective cooling system for electronic devices, etc. Mathematically computed expressions for Nusselt number (Nu_{x_1}) and Skin friction coefficient (C_f) are defined as [50–52]

Fig. 2 Working flowchart



$$Nu_{x_1} = \frac{\left[K_{hnf} \left(-\frac{\partial T_1}{\partial y_1} \right) + q_r \right]_{@y_1=0}}{K_f(T_{1_w} - T_{1_\infty})/2L}$$

$$= \frac{\left[K_{hnf} \left(-\frac{\partial T_1}{\partial y_1} \right) + \frac{4\sigma^*}{3K^*} \left(-\frac{\partial T_1^4}{\partial y_1} \right) \right]_{@y_1=0}}{K_f(T_{1_w} - T_{1_\infty})/2L} \text{ and} \tag{14}$$

$$C_f = \frac{\mu_{hnf}}{\rho_f u_{1_w}^2} \left(\frac{\partial u_1}{\partial y_1} \right)_{@y_1=0} \tag{15}$$

By using the Eq. (7), Eq's (13) - (14), ([53, 54]) are transformed as follows

$$Re_{x_1}^{-1/2} Nu_{x_1} = - \left[\frac{K_{hnf}}{K_f} + Nr_1 \right] \text{ and} \tag{16}$$

$$Re_{x_1}^{1/2} C_f = - \frac{\mu_{hnf}}{\mu_f} f_1''(0),$$

where $Re_{x_1} = \frac{u_{1_w}(x_1)x_1}{\nu_f}$ represents Reynolds number.

Figure 2 provides the pictorial representation (Flowchart) of present study step by step which includes transmission of PDE's system into ODE's system on employing suitable similarity transformation and then using MATLAB bvp4c numerical solver. Functions generated a code to compile the momentum, thermal, heat transmission and skin friction coefficients results at various values of emerging parameters of current numerical computation.

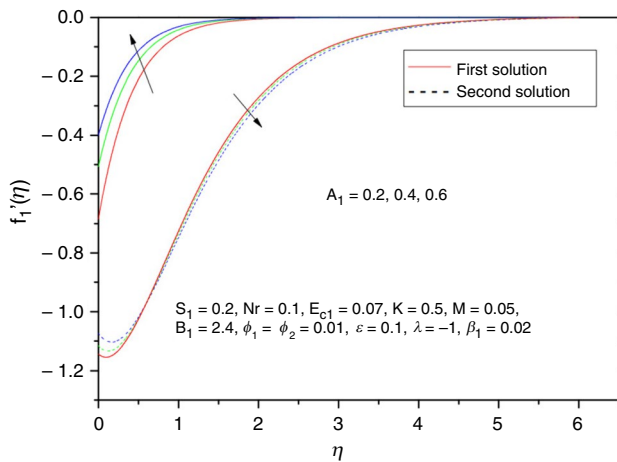


Fig. 3 Velocity profile varying $A_1 = 0.2, 0.4, 0.6$

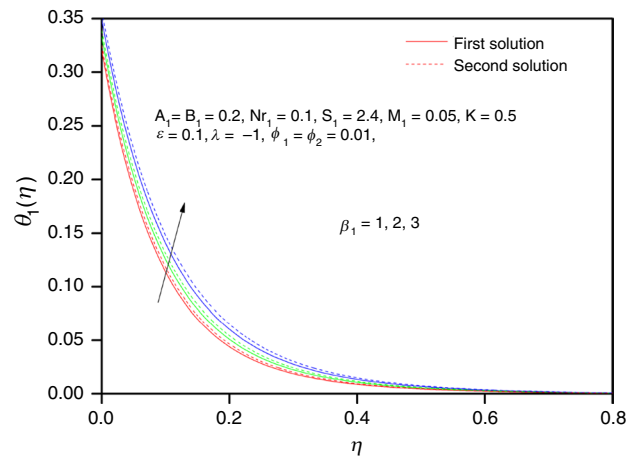


Fig. 5 Temperature profile varying $\beta_1 = 1, 2, 3$

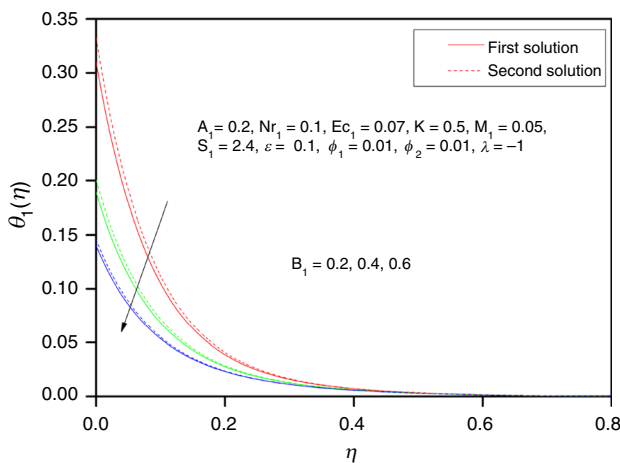


Fig. 4 Temperature profile varying $B_1 = 0.2, 0.4, 0.6$

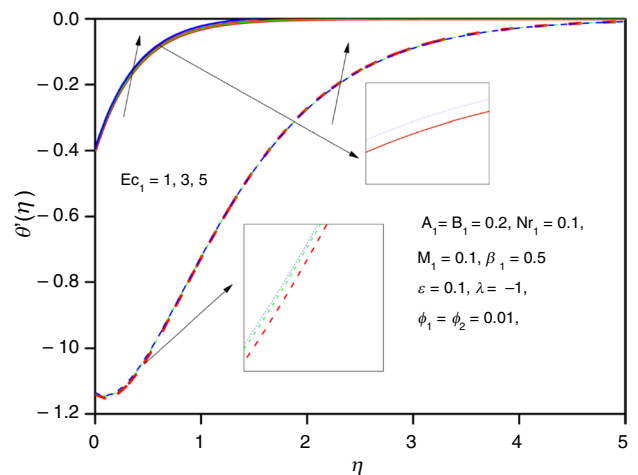


Fig. 6 Velocity profile varying $Ec_1 = 1, 3, 5$

Flow stability

It can be observed that for shrinking parameter, dual solutions exist. Therefore, stability analysis is performed to inspect whether the solution is stable with respect to time and physically reliable. [63] concluded that first branch solution is physically reliable on the contrary second branch solution are not physically reliable. To investigate the flow stability, numerical simulation is employed introducing a time dependent form of Eq's. (2-3) in Eq's (8-9), respectively

$$\left(\frac{\mu_{hnf}/\mu_f}{\rho_{hnf}/\rho_f}\right) \frac{\partial^3 f_1}{\partial \eta^3} + f \frac{\partial^2 f_1}{\partial \eta^2} - 2 \left(\frac{\partial f_1}{\partial \eta}\right)^2 - \frac{\partial^2 f_1}{\partial \eta \partial \tau} - \left(\frac{\sigma_{hnf}/\sigma_f}{\rho_{hnf}/\rho_f}\right) M_1 \frac{\partial f_1}{\partial \eta} - \left(\frac{\mu_{hnf}/\mu_f}{\rho_{hnf}/\rho_f}\right) K \frac{\partial f_1}{\partial \eta} = 0. \tag{17}$$

$$\frac{1}{Pr_1} \left[\left(\frac{K_{hnf}}{K_f} (1 + \epsilon \theta_1) + Nr_1 \right) \frac{\partial^2 \theta_1}{\partial \eta^2} + \frac{K_{hnf}}{K_f} \epsilon \left(\frac{\partial \theta_1}{\partial \eta} \right)^2 \right] + \frac{(\rho C_p)_{hnf}}{(\rho C_p)_f} \left[\frac{\partial \theta_1}{\partial \eta} f_1 - \frac{\partial f_1}{\partial \eta} \theta_1 - \frac{\partial \theta_1}{\partial \tau} \right] + \beta_1 \theta_1 + \frac{\mu_{hnf}}{\mu_f} Ec_1 \frac{\partial^2 f_1}{\partial \eta^2} = 0. \tag{18}$$

with boundary conditions

$$f_1(0, \tau) = S_1, \quad \frac{\partial f_1}{\partial \eta}(0, \tau) = \lambda + A_1 \frac{\partial^2 f_1}{\partial \eta^2}(0, \tau), \tag{19}$$

$$\theta_1(0, \tau) = 1 + B_1 \frac{\partial \theta_1}{\partial \eta}(0, \tau)$$

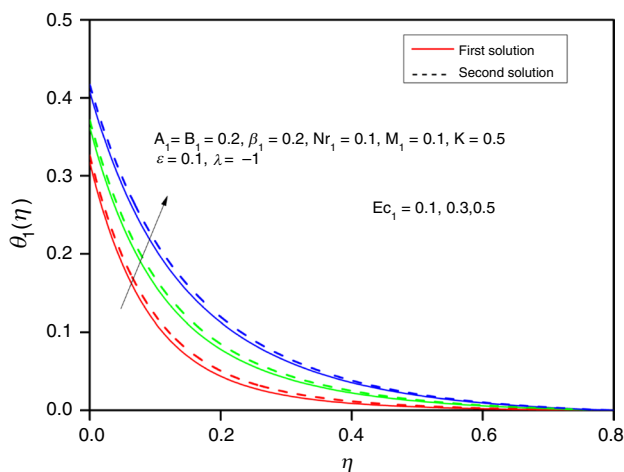


Fig. 7 Temperature profile varying $Ec_1 = 0.1, 0.3, 0.5$

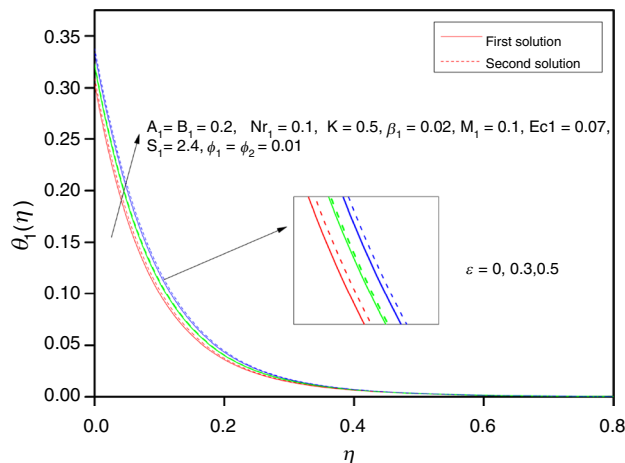


Fig. 8 Temperature profile varying $\epsilon = 0, 0.3, 0.5$

$$\frac{\partial f_1}{\partial \eta}(\infty, \tau) \rightarrow 0, \theta_1(\infty, \tau) \rightarrow 0. \tag{20}$$

The system perturbation equations are significant from where stability is tested, and positive or negative sign of the smallest eigenvalue δ_1 determine stability of the outcomes. Using this theory of stability, $f_0(\eta) = f_1(\eta)$, $\theta_0(\eta) = \theta_1(\eta)$, and δ is a set of eigenvalues where $\delta_1 < \delta_2 < \delta_3 < \dots < \delta_{n-1} < \delta_n$.

Let perturbation equations be ([55])

$$f_1(\eta, \tau) = f_0(\eta) + e^{-\delta\tau} F_1(\eta), \theta_1(\eta, \tau) = \theta_0(\eta) + e^{-\delta\tau} G_1(\eta), \tag{21}$$

where, $F_1(\eta)$ and $G_1(\eta)$ are small respective to $f_0(\eta)$ and $\theta_0(\eta)$, and δ represents eigenvalue parameter that is to be evaluated.

Adopting Eq. (21) into Eq's (17–20) and set the value of τ to zero, and linearized eigenvalue problem is taken as

$$\left(\frac{\mu_{hnf}}{\rho_{hnf}}\right) F_1''' + F_1 f_0'' + F_1' f_0' - 4f_0 F_1' + \delta F_1' - \left(\frac{\sigma_{hnf}}{\rho_{hnf}}\right) M_1 F_1' + \left(\frac{\mu_{hnf}}{\rho_{hnf}}\right) K F_1' = 0, \tag{22}$$

$$\frac{1}{Pr_1} \left[\left(\frac{K_{hnf}}{K_f}\right) (1 + \epsilon\theta_0) + Nr_1 \right] G_1'' + \frac{K_{hnf}}{K_f} \epsilon (G_1')^2 + \frac{(\rho C_p)_{hnf}}{(\rho C_f)} [F_1 \theta_1' + G_1' f_0 - F_1' \theta_0 - G_1 f_0' + \delta G_1] + \beta_1 G_1 + \frac{\mu_{hnf}}{\mu_f} Ec_1 F_1 f_0'' = 0. \tag{23}$$

with corresponding boundary conditions

$$F_1(0) = 0; F_1'(0) = A_1 F_1''(0); G_1(0) = B_1 G_1'(0), \tag{24}$$

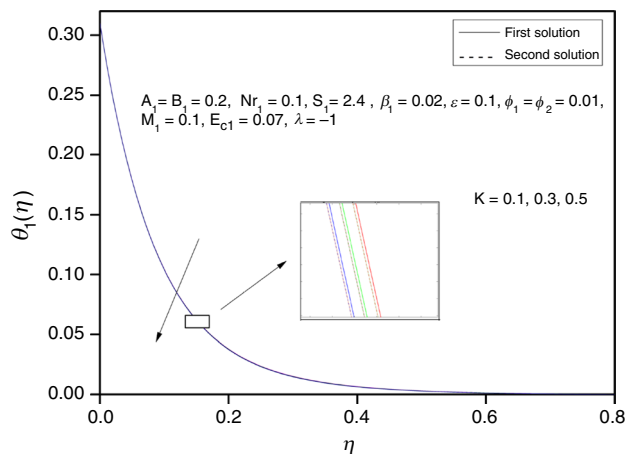


Fig. 9 Temperature profile varying $K = 0.1, 0.3, 0.5$

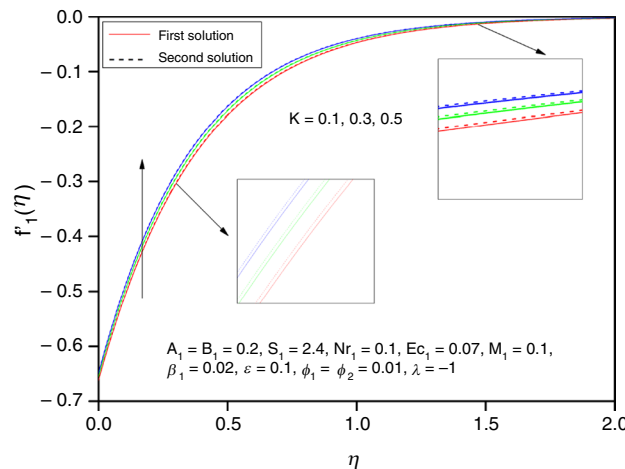


Fig. 10 Velocity profile varying $K = 0.1, 0.3, 0.5$

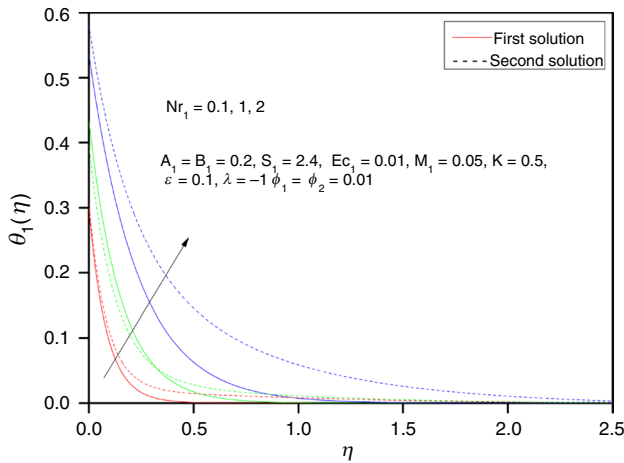


Fig. 11 Temperature profile varying $Nr_1 = 0.1, 1, 2$

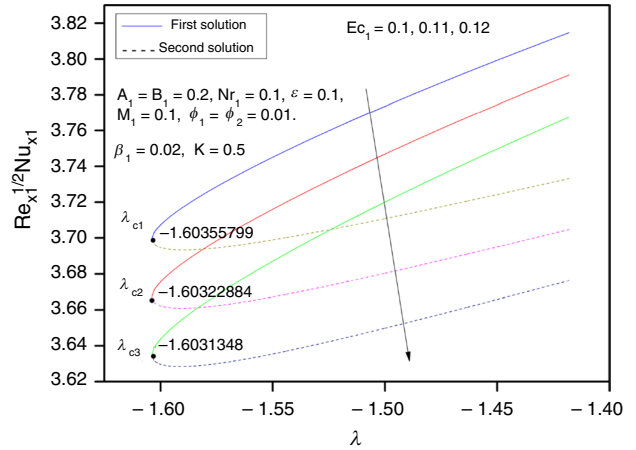


Fig. 14 Influence of λ on $Nu_{x,1}$, Varying $Ec_1 = 0.1, 0.11, 0.12$

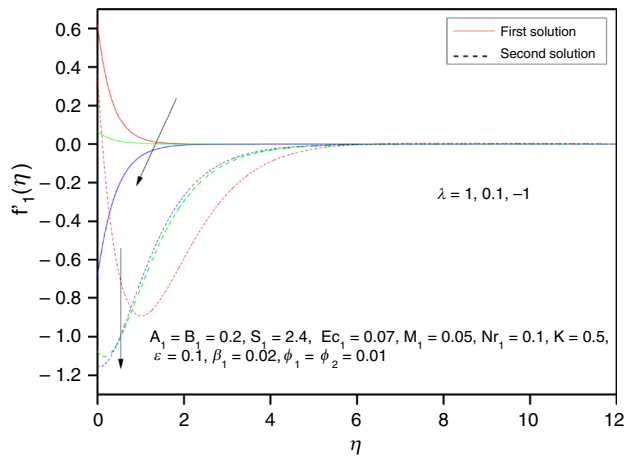


Fig. 12 Velocity profile varying $\lambda = 0.1, 1, 2$

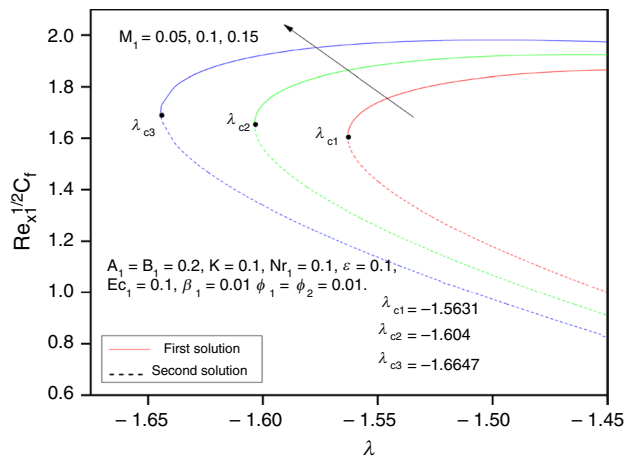


Fig. 15 Influence of λ on C_f , Varying $M_1 = 0.05, 0.1, 0.15$

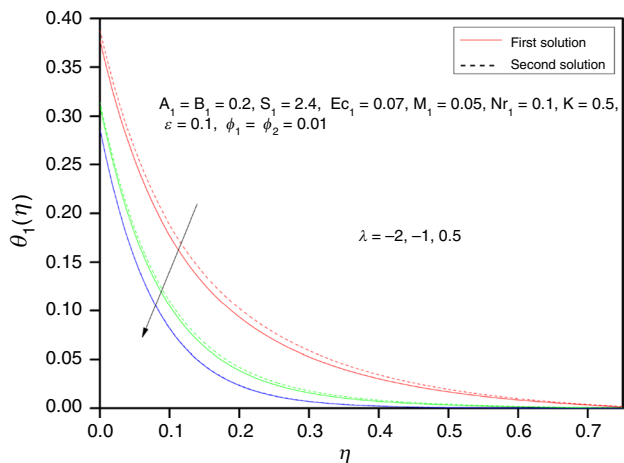


Fig. 13 Temperature profile varying $\lambda = -2, -1, 0.5$

$$F_1'(\infty) \rightarrow 0; G_1(\infty) \rightarrow 0. \tag{25}$$

Using Eq. (19), the unsteady state outcome $f_1(\eta, \tau)$ converges to the steady-state outcome $F_1(\eta)$ as $\tau \rightarrow \infty$ if $\delta > 0$. [56] retrieved boundary conditions with a new one to possess a non-trivial outcome eigenvalue to get justified values of δ . In the current numerical simulation, $F_1'(\infty) \rightarrow 0$ is retrieved with $F_1''(0) = 1$. A bvp4c function in MATLAB is used to obtain the δ -unknown values and to ascertain the hybrid nano liquid flow stability $\delta_1 > 0$ implies that the outcome is real and stable whereas negative value of smallest eigenvalues concludes that the solution is not realistic.

Table 1 Values for varied ϕ_1 with $A_1 = B_1 = 0.2, \beta_1 = 0.02, K = 0.5, S_1 = 2.4, M_1 = Ec_1 = \epsilon = Nr_1 = 0.1, \lambda = -1.5, \phi_2 = 0.01$

ϕ_1	Nu_{x_1}		c_f	
	First Outcome	Second Outcome	First Outcome	Second Outcome
0.01	3.779456923	3.508352265	2.255471505	0.474538561
0.02	3.833533045	3.544390942	2.314695478	0.485754091
0.03	3.886707709	3.578878470	2.373933845	0.498572351

Results and discussion

Tables 1–7 explores the Nusselt and Skin friction values with different parameter values whereas Tables 8–10 describes the comparison of present outcomes with existing investigation to conclude the excellence of the current development of the research article. Tables 11–13 provides the properties of water and nanoparticles which are used to obtain the behavior of hybrid nanofluids ($H_2O-Cu-Al_2O_3$). Nanoparticles thermal conductivity influences the improvement in the thermal conductivity of the nano liquid. Base fluid H_2O has high thermal conductivity compared to the other base fluids. Adding nanoparticles Cu and Al_2O_3 which have high and good thermal conductivity contributes to intensify heat transfer performance of hybrid nanofluid. The results section describes the significance of computed outcomes and presents the analysis of momentum, thermal, heat transfer and skin friction characteristics and also analyses the nature of duality of solutions of hybrid nano liquid ($Cu - Al_2O_3 - H_2O$) with fixed Prandtl number, $Pr_1 = 6.2$ in this complete study. MATLAB software helped to perform the numerical computation using bvp4c function. Figures 3–15 shows the existence of two solutions (First and Second) with respect to the boundary conditions for certain values of λ , which depends on the S-strength. At $\lambda = \lambda_c$ the outcomes bifurcate, where $\lambda_c =$ critical value of λ . Hence, to observe dual solutions nature, initial guesses are taken in two sets and $\eta \rightarrow \infty$ as 15 with the values of pertinent parameters. Figure 3 refers to the profile of velocity stencil for enhancing values in momentum slip parameter ($A_1 = 0.2, 0.4, 0.6$) for both the solutions where first solution in solid lines reveals that momentum is an increasing function and second solution in dotted lines, is a deceleration function. Physically, it is anticipated owing to the positive fluid velocity gradient adjacent to the plane that leads to thinning of momentum boundary layer. Further, presence of momentum slip forces the more fluid to slip at the surface of the shrinking plane by decreasing the fluid resistance, and enhancing momentum flow; thus, an elevated degree of velocity slip is needed to intensify flow velocity and vice versa. For pivot values of $A_1 = 0.1, 0.2, 0.4$ which are in increasing order as explored in Table 3, it is viewed that

heat transmission coefficient elevates whereas skin friction coefficient drops for both I and II outcomes. It is seen that 1st outcome is more stable compared to the 2nd outcome for both coefficients of heat transmission and skin friction. It is since, fluid velocity enhancement results an amplification in fluid motion which leads to an increase in rate of heat transmission between the plane and liquid. When the motion of fluid is upsurges, the convection currents are stronger leading amplification in heat transfer coefficient.

Table 2 Values for varied ϕ_2 with $A_1 = B_1 = 0.2, \beta_1 = 0.02, K = 0.5, S_1 = 2.4, M_1 = Ec_1 = \epsilon = Nr_1 = 0.1, \lambda = -1.5, \phi_1 = 0.01$

ϕ_2	Nu_{x_1}		c_f	
	First Outcome	Second Outcome	First Outcome	Second Outcome
0.01	3.779456923	3.508352265	2.255471505	0.474538561
0.02	3.836590942	3.523548651	2.410918961	0.434142832
0.03	3.893056011	3.534208880	2.563270807	0.392785456

Table 3 Values for varied A_1 with $B_1 = 0.2, \beta_1 = 0.02, K = 0.5, S_1 = 2.4, Ec_1 = 0.03, M_1 = \epsilon = Nr_1 = 0.1, \lambda = 1.5, \phi_1 = \phi_2 = 0.01$

A_1	Nu_{x_1}		c_f	
	First Outcome	Second Outcome	First Outcome	Second Outcome
0.01	3.917408978	3.843704498	2.380747195	0.608031380
0.02	3.969183360	3.848829559	2.255470065	0.475393552
0.04	4.030373451	5.614962599	1.865874301	1.851983078

Table 4 Values for varied B_1 with $A_1 = 0.2, \beta_1 = 0.01, K = 0.5, S_1 = 2.4, Ec_1 = 0.01, M_1 = \epsilon = Nr_1 = 0.1, \lambda = -1.5, \phi_1 = \phi_2 = 0.01$

B_1	Nu_{x_1}	
	First Outcome	Second Outcome
0.02	4.024013354	3.947171209
0.04	2.373314008	2.341794765
0.06	1.681521623	1.663193667

Table 5 Values for varied S_1 with $A_1 = 0.2, \beta_1 = 0.02, K = 0.5, S_1 = 2.4, Ec_1 = 0.1, M_1 = 0.05, \epsilon = Nr_1 = 0.1, \lambda = -1.5, \phi_1 = \phi_2 = 0.01$

S_1	Nu_{x_1}	
	First Outcome	Second Outcome
2.30	3.702613892	3.3513361801
2.35	3.741898171	3.530197024
2.40	3.778972445	3.546117991

Table 6 Values for varied ϵ with $A_1 = B_1 = 0.2$, $\beta_1 = 0.02$, $K = 0.5$, $Ec_1 = 0.01$, $M_1 = 0.01$, $S_1 = 2.4$, $Nr_1 = 0.1$, $\lambda = -1.5$, $\phi_1 = \phi_2 = 0.01$

ϵ	Nu_{x_1}	
	First Outcome	Second Outcome
0.05	4.040724879	3.964892247
0.10	4.023594399	3.947817761
0.15	4.006119109	3.925755461

Table 7 Values for varied Nr_1 with $A_1 = 0.4$, $B_1 = 0.2$, $\beta_1 = 0.01$, $K = 0.5$, $Ec_1 = 0.01$, $M_1 = 0.05$, $S_1 = 2.2$, $\epsilon = 0.1$, $\lambda = -2$, $\phi_1 = \phi_2 = 0.005$

Nr_1	Nu_{x_1}	
	First Outcome	Second Outcome
0.1	3.786516264	3.816049415
0.2	4.023152779	3.996955597
0.3	4.272616154	4.208260611

In Fig. 4, variation in thermal profiles for different values of thermal slip parameter is delineated. From the figure, it is concluded that with the rise in thermal slip parameter ($B_1 = 0.2, 0.4, 0.6$) at the shrinking plane ($\lambda = -1$ and -1.5 , respectively) thermal boundary layer thickness decreases even when only a small amount of heat is transferred to the plane by the fluid. Effect of thermal slip parameter on the Nusselt number is presented in the Table 4. From the numerical values, it is well established that increase in the thermal slip parameter slows down the heat transfer mechanism. On the other hand, rise in thermal distribution as heat source/sink parameter (which depends on amount of heat source/sink in the liquid) ($\beta_1 = 1, 2, 3$) improves is shown in Fig. 5. It is also viewed that the first outcome plotted in solid lines is lower than that of second solution plotted in dotted lines. It is real, since upsurge in thermal slip parameter causes an elevation in the rate of heat transmission with a decrement in thermal stencil.

Figure 6 portrays that velocity upsurgers as Eckert number ($Ec_1 = 1, 3, 5$) rises for both upper (first) branch and lower (second) branch. For higher values of viscous dissipation parameter Ec , velocity reaches to -0.37809604

Table 9 Comparison of $-\theta_1(0)$ for viscous fluid ($\phi_1 = \phi_2 = 0$) when $S_1 = 3$, $Nr_1 = S_1 = A_1 = B_1 = \beta_1 = 0$ for stretching plane ($\lambda = 1$)

Pr_1	M_1	EL Aziz [57]	Ishak [58]	Waini [60]	Present Results
0.5	0	0.594493		0.594339	0.59668759
1.0	0	0.954785	0.9548	0.954783	0.95481061
2.0	0		1.4715	1.471460	1.47146137
3.0	0	1.869074	1.8681	1.869074	1.869087481
5.0	0	2.500132		2.500132	2.500133544
10.0	0	3.660372		3.660372	3.660369315
1.0	1		0.8611	0.861984	0.861508655

for upper branch (first) solution and -1.14675653 for lower branch (second) solution and there by increases reaching to its free stream at $Ec_1 = 5$. Figure 7 describes the variation in thermal profile for $Ec_1 (= 0.1, 0.3, 0.5)$. It is an important factor for studying the thermal profile of the fluid flow. It is noticed that temperature distribution rises as Ec_1 enhances. At $Ec_1 = 0.5$, temperature reaches to 0.401713002 , for first solution as exposed in solid lines and temperature reaches to 0.408873912 , for second solution as explored in dotted lines. Physically, it is true since Eckert number is measure of thermal energy dissipated during the conversion of kinetic energy of fluid molecules to thermal energy. This energy conversion releases the heat to the system, and hence enhances the temperature. An upsurge in thermal conductivity due to enhancement in temperature speed up the thermal conduction from the surface into the liquid, causes thermal stencil to grow and Nu_{x_1} reduce as variable thermal conductivity parameter $\epsilon (= 0, 0.3, 0.5)$ amplifies as depicts in Fig. 8 and Table 6.

Figures 9 and 10 captures the temperature and momentum behavior of thermal conductivity of hybrid nano liquid. An improvement in velocity profile is noticed, whereas a reverse trend in temperature stencil is noticed with enhancement in $K (= 0.1, 0.3, 0.5)$. Since, the nanoparticle temperature rises, the internal particle velocity grows and transfers heat with less resistance causes decrease in thermal profile.

The thermal variation for different enhanced values of thermal radiation $Nr_1 (= 0.1, 1, 2)$ is seen in Fig. 11. It manifests that temperature is an accelerating function of $Cu - Al_2O_3 - H_2O$. The physical reason behind this is an

Table 8 Comparison of $f_1''(0)$ and $-\theta_1'(0)$ for viscous fluid ($\phi_1 = \phi_2 = 0$) when $S_1 = 3$, $Pr_1 = 0.7$, $M_1 = Nr_1 = A_1 = B_1 = \beta_1 = \epsilon = 0$ for shrinking sheet ($\lambda = -1$)

Existing Literature	$f_1''(0)$		$-\theta_1'(0)$	
	First Outcome	Second Outcome	First Outcome	Second Outcome
Ghosh and Mukhopadhyay [61]	2.39082	-0.97223	1.7710	0.84838
Waini, Ishak, and Pop [60]	2.390814	-0.972247	1.771237	0.848316
Gopinath Mandal and Dulal Pal [25]	2.390814	-0.97218	1.771238	0.847849
Present Outcomes	2.390813634	-0.972247455	1.771237307	0.848315747

Table 10 Comparison of Least Eigenvalues

A_1	λ	γ_1, γ_2 [59]		γ_1, γ_2 [25]		Current Outcomes	
		I Outcome	II Outcome	I Outcome	II Outcome	I Outcome	II Outcome
0.2	-1.441	0.6126	0.06126485	-0.06119732	0.06126486	-0.06119732	
	-1.448	0.01326	-0.01326	0.01325891	-0.01325575	0.01325891	-0.01325576
0.4	-2.03	0.134477	-0.02518	0.13445924	-0.13450106	0.13445928	-0.1345011
	-2.036	0.00711	-0.00713	0.00712339	-0.00712348	0.00712338	-0.00712348

Table 11 Thermophysical properties of nanofluid and hybrid nanofluid [25]

Properties	Nanofluid	Hybrid Nanofluid
Density	$\frac{\rho_{nf}}{\rho_f} = (1 - \phi_1) + \phi_1 \frac{\rho_{s1}}{\rho_f}$	$\frac{\rho_{hnf}}{\rho_f} = \left[(1 - \phi_2) + \phi_1 \frac{\rho_{s1}}{\rho_f} \right] + \phi_2 \frac{\rho_{s2}}{\rho_f}$
Heat Capacitance	$\frac{(\rho C_p)_{nf}}{(\rho C_p)_f} = (1 - \phi_1) + \phi_1 \left[\frac{(\rho C_p)_{s1}}{(\rho C_p)_f} \right]$	$\frac{(\rho C_p)_{hnf}}{(\rho C_p)_f} = (1 - \phi_2) \left[(1 - \phi_1) \left[\frac{(\rho C_p)_{s1}}{(\rho C_p)_f} \right] \right] + \phi_2 \left[\frac{(\rho C_p)_{s2}}{(\rho C_p)_f} \right]$
Dynamic Viscosity	$\frac{\mu_{nf}}{\mu_f} = \frac{1}{(1 - \phi_1)^{2.5}}$	$\frac{\mu_{hnf}}{\mu_f} = \frac{1}{(1 - \phi_1)^{2.5} (1 - \phi_2)^{2.5}}$
Electrical Conductivity	$\frac{\sigma_{nf}}{\sigma_f} = 1 - \frac{3\phi_1 \left(1 - \frac{\sigma_{s1}}{\sigma_f} \right)}{\left(2 + \frac{\sigma_{s1}}{\sigma_f} \right) + \phi_1 \left(1 - \frac{\sigma_{s1}}{\sigma_f} \right)}$	$\frac{\sigma_{hnf}}{\sigma_f} = 1 - \frac{3\phi_2 \left(1 - \frac{\sigma_{s2}}{\sigma_{nf}} \right)}{\left(2 + \frac{\sigma_{s2}}{\sigma_{nf}} \right) + \phi_2 \left(1 - \frac{\sigma_{s2}}{\sigma_{nf}} \right)}$; $\frac{\sigma_{hnf}}{\sigma_f} = \frac{\sigma_{nf}}{\sigma_f} \times \frac{\sigma_{hnf}}{\sigma_{nf}}$
Thermal Conductivity	$\frac{K_{nf}}{K_f} = \frac{K_{s1} + 2K_f - 2\phi_1(K_f - K_{s1})}{K_{s1} + 2K_f + \phi_1(K_f - K_{s1})}$	$\frac{K_{hnf}}{K_{nf}} = \frac{K_{s2} + 2K_{nf} - 2\phi_2(K_{nf} - K_{s2})}{K_{s2} + 2K_{nf} + \phi_2(K_{nf} - K_{s2})}$; $\frac{K_{hnf}}{K_f} = \frac{K_{hnf}}{K_{nf}} \times \frac{K_{nf}}{K_f}$
Variable Thermal Conductivity	$K_{hnf}^*(T) = K_{hnf} \left(1 + \epsilon \frac{T_1 - T_{1\infty}}{T_{1w} - T_{1\infty}} \right)$	

Table 12 Numerical values of various properties for base fluid and nanoparticles [25]

Properties	Base fluid H ₂ O	Nano Particles	
		Cu	Al ₂ O ₃
Density (ρ) (Kg m ⁻³)	997.1	8933	3970
Thermal Conductivity (K) (W m ⁻¹ K ⁻¹)	0.613	400	40
Specific Heat (C _p) (JKg ⁻¹ K ⁻¹)	4179	385	765
Electrical Conductivity (σ)	0.05	5.96 × 10 ⁴	35 × 10 ⁴

increment in thermal radiation diminishes the Rosseland radiative absorption and, consequently, the radiative heat flux results amplification in the thermal boundary layer thickness.

Figures 12 and 13 manifests the distributions of momentum and thermal varying Stretching sheet/Shrinking sheet parameter $\lambda (= 1, 0.1, -1)$ for hybrid nanofluid. When $\lambda = 1$, velocity of $Cu - Al_2O_3 - H_2O$ accelerate. This is because by stretch, which decelerate viscous effect on fluid flow causing momentum to enhance. For $\lambda = -1$, momentum of $Cu - Al_2O_3 - H_2O$ diminishes, when the shrinking parameter is increased. Since, the resistance to movement of the flow due high viscosity causes velocity not to enhance.

The temperature of fluid with stretch in $\lambda (= -2, -1, 0.5)$, shrinks because stretching surface intensify hybrid nanofluid velocity which in turn enhances thermal boundary layer thickness causes reduction in the thermal stencil.

The effect of heat transfer and skin friction coefficient for varied values of Ec_1 and M_1 are exemplified in Figs. 14 and 15, respectively. The presence of dual solution is noticed for $Ec_1 (= 0.1, 0.11, 0.12)$ when the critical value of $(\lambda = \lambda_c)$ are $\lambda_{c_1} = -1.60355799$, $\lambda_{c_2} = -1.60322884$ and $\lambda_{c_3} = -1.6031348$, respectively. It is seen that heat transfer coefficient Nu_{x_1} enlarge as Ec_1 rises gradually. An improvement in Ec_1 causes the transformation of kinetic energy into internal energy by work that is done against

Table 13 Enhancement in heat transmission of fluids using different nanoparticles [62]

Base Fluid	Nanoparticle	Development in Conductance	Volume Concentration
Water - H ₂ O	Cu	34%	0-16%
Water - H ₂ O	Al ₂ O ₃	31%	0-18%

the viscous fluid stresses. Due to this, temperature of the hybrid nano liquid increases as Ec_1 increases. The skin friction variation with magnetic field M_1 ($= 0.05, 0.1, 0.15$) is captured with $\lambda = [-1.65, -1.45]$, and critical values are viewed at $\lambda_{c_1} = -1.5631$, $\lambda_{c_2} = -1.604$ and $\lambda_{c_3} = -1.6647$.

The influence of enhanced volume fraction of copper nanoparticle ϕ_1, ϕ_2 ($= 0.01, 0.02, 0.03$) on heat transfer and skin friction coefficient in Tables 1 and 2 is viewed to improve and more convergent than the second solution of hybrid nano liquid. From this observation, we can say that first solution is more stable than the second solution with $A_1 = B_1 = 0.2, \beta_1 = 0.02, K = 0.5, S_1 = 2.4, M_1 = Ec_1 = 0.01, \epsilon = Nr_1 = 0.1, \lambda = -1.5$ and $\phi_2 = \phi_1 = 0.01$, respectively. It is true because the presence of hybrid nanoparticles can disrupt by altering the flow pattern of thermal boundary layer which leads to elevate the rate of heat transfer and skin friction coefficient. As slip velocity is the relative velocity between the fluid and the solid surface, it affects both heat transfer and skin friction coefficient. An enhancement in the velocity slip parameter implies a larger slip velocity at the wall, reduce the shear stress at the wall which leads to decelerate the coefficient of skin friction and accelerate the coefficient of heat transfer as portrayed in Table 3. Table 4 depicts the reduction in Nusselt number with rise in thermal slip parameter. An increase in thermal slip parameter results a reduction in the temperature gradient at the fluid to solid interface and it implies less effective thermal boundary layer in transferring heat from solid surface to the fluid. As a consequence, the convective heat transfer is reduced which leads the Nusselt number to reduce. Tables 5 and 7 exhibit the impact of S_1 and Nr_1 on Nu_{x_1} as intensifying values as both parameters enhance, respectively. Heat transmission coefficients amplify as suction parameter amplifies with a fact that in enhancement in suction, thermal profile diminishes and gradient of temperature rises, so the convection coefficient of heat transfer which depends on thermal gradient grows, improving the Nusselt number accordingly. Maximum values of Nu_{x_1} noticed as 3.778972445 at upper branch and 3.546117991 at lower branch when $S_1 = 2.4$ and $\lambda = -1.5, 4.272616154, 4.208260611$ when $Nr_1 = 0.3$ and $\lambda = -2$, at first and second outcomes of $Cu - Al_2O_3 - H_2O$. The least eigen values for preferred values of A_1 and λ with $S_1 = 2.4$,

$Nr_1 = M_1 = Ec_1 = 0, \phi_1 = \phi_2 = 0.01, B_1 = 0.2, \beta_1 = 0.02$ is discussed in Table 9 and found to be accurate with existing investigation [25, 59].

The comparison Tables 8 and 9 expose that the present numerical simulation is excellent when compared with existing literature [25, 48, 61] for and when viscous liquid ($\phi_1 = \phi_2 = 0$), $S_1 = 3, Pr_1 = 0.7$, and $M_1 = Nr_1 = A_1 = B_1 = \beta_1 = \epsilon = 0$ for $\lambda = -1$ and [57, 58, 60] varying with $Pr_1 = 0.5, 1, 2, 3, 5, 10$ and $M_1 = 0, 1$ for (dual results) when viscous liquid ($\phi_1 = \phi_2 = 0$), $S_1 = 3$, and $Nr_1 = S_1 = A_1 = B_1 = \beta_1 = \epsilon = 0$ for $\lambda = 1$. As *bvp4c* is mainly computed with initial guess for the dependent variable at the left boundary and often for the derivatives of the dependent variable w.r.t. the independent variable, we assume that the initial guess taken in the present simulation makes excellence with the existing investigation as cited above.

Conclusions

The outcomes of a MHD hybrid nano liquid slip flow of thermal radiation with influence of viscous dissipation over an exponentially stretching/shrinking plane is numerically explored using a MATLAB solver and are elevated as below:

- The existence of expandable/diminishing surface, as well as a sufficient amount of suction, helps in occurrence of dual solutions, and found that upper branch is stable.
- Nanoparticles of copper and alumina elevate the effectiveness of heat transmission in dual solutions.
- As suction parameter enhances Nu_{x_1} elevates, whereas reverse trend is noticed C_f in both first and second solutions.
- The elevation in velocity slip parameter, explores the intensification of momentum distribution, for first outcome and reverse phenomena for second outcome, Nu_{x_1} intensifies as A_1 elevates.
- Enhancement in Ec_1 describes the improvement in both momentum and thermal profiles as well as the heat transmission coefficient with critical values $-1.60355799, -1.60322884, -1.6031348$.
- The temperature profile with increase in thermal slip factor is viewed to drop whereas enhancement is noticed with rise in heat generation/absorption parameter and variable thermal conductivity parameter, since temperature slip causes an elevation in heat transfer with a deceleration in thermal profile.
- Velocity profile is observed to elevate as stretching/shrinking surface parameter improves whereas the thermal profile is captured to diminish.
- The current study is viewed to be excellent when compared with existing literature and can be further

extended for mixed convection with non-similarity transformation.

- Due the presence of viscous dissipation, heat transfer rate decreases by 7.17% for first solution and 1.3% for second solution, and there is no change in C_f due to Eckert number, because Ec_1 is not directly associated with momentum equation. Heat transfer and C_f increases by 3.07% and 10.82%, respectively for first solution, whereas Nu_{x_1} increases by 1.69% for first solution and C_f decrease by 6.11% for second solution.

The future scope of the present article is useful to elevate the several attributes of three-dimensional flow in mixed convection of hybrid nanofluid through advanced computing techniques based on machine learning.

Acknowledgements First author would like to thank KLEF for providing fulltime fellowship for research work and we are also grateful to Editors and Reviewers for their valuable suggestions.

Declarations

Conflict of interest The authors declare that they have no competing interest.

References

1. Stephen Choi US, Eastman JA. Enhancing thermal conductivity of fluids with nanoparticles. San Francisco, CA: ASME Int Mech Engg Cong and Exp; 1995.
2. Khan WA, Pop I. Boundary layer flow of a nanofluid past a stretching sheet. *Int J of Heat and Mass Tran.* 2010;53:2477–83. <https://doi.org/10.1016/j.ijheatmasstransfer.2010.01.032>.
3. Makinde OD, Aziz A. Boundary layer flow of a nanofluid past a stretching sheet with a convective boundary condition. *Int J of Ther Sci.* 2011;50(7):1326–32. <https://doi.org/10.1016/j.ijthermalsci.2011.02.019>.
4. Rana P, Bhargava R. Flow and heat transfer of a nanofluid over a nonlinearity stretching sheet: A numerical study. *Comm in Nonlin Sci and Num Sim.* 2012;17(1):212–26. <https://doi.org/10.1016/j.cnsns.2011.05.009>.
5. Khan WA, Makinde OD. MHD nanofluid bioconvection due to gyrotactic microorganisms over a convectively heat stretching sheet. *Int J of Ther Sci.* 2014;81:118–24. <https://doi.org/10.1016/j.ijthermalsci.2014.03.009>.
6. Rajesh V, Anwar Beg O, Mallesh MP. Transient nanofluid flow and heat generation from a moving vertical cylinder in the presence of thermal radiation: Numerical Study. *J of Nanoengng and Nanosys.* 2014;230(1):1–14. <https://doi.org/10.1177/1740349914548712>.
7. Rajesh V, Chamkha A, Mallesh MP. Nanofluid flow past an impulsively started vertical plate with variable surface temperature. *Int J of Num Met for Heat and Fluid Flow.* 2016;26(1):328–47. <https://doi.org/10.1108/HFF-07-2014-0209>.
8. Rajesh V, Chamkha AJ, Mallesh MP. Transient MHD Free Convection Flow and Heat Transfer of Nanofluid past an Impulsively Started Semi-Infinite Vertical Plate. *J of App Fluid Mech.* 2016;9(5):2457–67. <https://doi.org/10.18869/ACADPUB.JAFM.68.236.23443>.
9. Kavitha M, Rajesh V, Mallesh MP, Chamkha AJ. Unsteady CNTs kerosene nanofluid flow past a vertical plate with heat transfer under the influence of thermal radiation. *AIP Conf Pro.* 2020;2246:1–9. <https://doi.org/10.1063/5.0014577>.
10. Kavitha M, Rajesh V, Mallesh MP. Numerical computation of CNTs water based nanofluid flow with heat generation/ absorption past an oscillating vertical plate with variable temperature. *AIP Conf Pro.* 2021;2316:1–9. <https://doi.org/10.1063/5.0036442>.
11. Dogonchi AS, Tayebi T, Chamkha AJ, Ganji DD. Natural convection analysis in a square enclosure with a wavy circular heater under magnetic field and nanoparticles. *J of Ther Ana and Cal.* 2020;139:661–71. <https://doi.org/10.1007/s10973-019-08408-0>.
12. Afshar SR, Mishra SR, Dogonchi AS, Karimi N, Chamkha AJ, Abulkhair H. Dissection of entropy production for the free convection of NEPCMs-filled porous wavy enclosure subject to volumetric heat source/sink. *J of Tai Inst of Chem Engg.* 2021;128:98–113. <https://doi.org/10.1016/j.jtice.2021.09.006>.
13. Dogonchi AS, Bondareva NS, Sheremet MA, El-Sapa S, Chamkha AJ, Shah NA. Entropy generation and heat transfer performance analysis of a non-Newtonian NEPCM in an inclined chamber with complicated heater inside. *J of Ene St, Vol 2023;72(partE):* <https://doi.org/10.1016/j.est.2023.108745>
14. Suresh S, Venkitaraj KP, Selvakumar P, Chandrasekar M. Effect of Al₂O₃-Cu/water hybrid nanofluid in heat transfer. *Exp Ther and Fluid Sci.* 2012;38(1):54–60. <https://doi.org/10.1016/j.expthermflusci.2011.11.007>.
15. Madhesh D, Kalaiselvam S. Experimental Analysis of Hybrid Nanofluid as a Coolant. *Pro Engg.* 2014;97(1):1667–75. <https://doi.org/10.1016/j.proeng.2014.12.317>.
16. Ghadikolaei SS, Yassari M, Sadeghi H, Hosseinzadeh Kh, Ganji DD. Investigation on thermophysical properties of TiO₂ – Cu/H₂O hybrid nanofluid transport dependent on shape factor in MHD stagnation point flow. *Pow Tech.* 2017;322(1):428–38. <https://doi.org/10.1016/j.powtec.2017.09.006>.
17. Iqbal Z, Azhar E, Maraj EN. Utilization of the computational technique to improve the thermophysical performance in the transportation of an electrically conducting Al₂O₃-Ag/H₂O hybrid nanofluid. *Eur Phy J Plus.* 2017;132(12):1–13. <https://doi.org/10.1140/epjp/i2017-11806-0>.
18. Rashad AM, Armaghani T, Chamkha AJ, Mansour MA. Entropy generation and MHD natural convection of a nanofluid in an inclined square porous cavity: Effects of a heat sink and source size and location. *Chi J of Phy.* 2018;56(1):193–211. <https://doi.org/10.1016/j.cjph.2017.11.026>.
19. Shah TR, Ali HM. Applications of hybrid nanofluids in solar energy, practical limitations and challenges: A critical review. *Sol Ene.* 2019;183(1):1173–203. <https://doi.org/10.1016/j.solener.2019.03.012>.
20. Shoaib M, Asif Zahoor Raja M, Touseef Sabir M, Islam Saeed, Shah Zahir, Kumam Poom, Alrabaiah Hussam. Numerical investigation for rotating flow of MHD hybrid nanofluid with thermal radiation over a stretching sheet. *Sci Rep.* 2020;10(1):1–15. <https://doi.org/10.1038/s41598-020-75254-8>.
21. Anusha T, Huang HN, Mahabaleshwar US. Two-dimensional unsteady stagnation point flow of Casson hybrid nanofluid over a permeable fat surface and heat transfer analysis with radiation. *J of the Tai Inst of Chem Engg.* 2021;127:79–91. <https://doi.org/10.1016/j.jtice.2021.08.014>.
22. Rajesh V, Kavitha M, Mallesh MP. Effects of MHD and Thermal Radiation on Unsteady Free Convective Flow of a Hybrid Nanofluid Past a Vertical Plate. *App Ana, Comp Math Mod Engg.* 2022;897:21–41.
23. Sarfraz Mahnoor, Yasir Muhammad, Khan Masood. Multiple solutions for non-linear radiative mixed convective hybrid

- nanofluid flow over an exponentially shrinking surface. *Sci Rep.* 2023;13(1):1–10. <https://doi.org/10.1038/s41598-023-29892-3>.
24. Sudarsana Reddy P, Sreedevi P, Chamkha Ali J. Hybrid nanofluid heat and mass transfer characteristics over a stretching/shrinking sheet with slip effects. *J Nanoflu.* 2023;12(1):251–60. <https://doi.org/10.1166/jon.2023.1996>.
 25. Mandal Gopinath, Pal Dulal. Stability analysis of radiative-magnetic hybrid nanofluid slip flow due to an exponentially stretching/shrinking permeable sheet with heat generation. *Int J of Amb Ene.* 2023. <https://doi.org/10.1080/01430750.2023.2173651>.
 26. Prakash Om, Rao PS, Sharma Ram Prakash, Mishra SR. Hybrid nanofluid MHD motion towards an exponentially stretching/shrinking sheet with the effect of thermal radiation, heat source and viscous dissipation. *Pramana J Phys.* 2023. <https://doi.org/10.1007/s12043-023-02533-0>.
 27. Nasir Saleem, Berrouk Abdallah S, Aamir Asim, Shah Zahir. Entropy optimization and heat flux analysis of Maxwell nanofluid configured by an exponentially stretching surface with velocity slip. *Sci Rep.* 2023. <https://doi.org/10.1038/s41598-023-29137-3>.
 28. Vanitha GP, Mahabaleshwar US, Xiaohu Hatami M, Yang X. Heat and mass transfer of micropolar liquid flow due to porous stretching/shrinking surface with ternary nanoparticles. *Sci Rep.* 2023;13(1):1–17. <https://doi.org/10.1038/s41598-023-29469-0>.
 29. Mallesh MP, Rajesh V, Kavitha M. Time-dependent thermal convective circulation of hybrid nanofluid past an oscillating porous plate with heat generation and thermal radiation. *J App Nonlin Dyn.* 2023;12(1):171–89. <https://doi.org/10.5890/JAND.2023.03.012>.
 30. Partha MK, Murthy PVS, Rajasekhar GP. Effect of viscous dissipation on the mixed convection heat transfer from an exponentially stretching surface. *Heat Mass Trans.* 2005;41(1):360–6. <https://doi.org/10.1007/s00231-004-0552-2>.
 31. Cortell Rafael. Flow and heat transfer of a fluid through a porous medium over a stretching surface with internal heat generation/absorption and suction/blowing. *Fluid Dyn Res.* 2005;37(4):231–45. <https://doi.org/10.1016/j.fluidyn.2005.05.001>.
 32. Mukhopadhyay S, Layek GC. Effects of thermal radiation and variable fluid viscosity on free convective flow and heat transfer past a porous stretching surface. *Int J Heat Mass Trans.* 2008;51(9–10):2167–78. <https://doi.org/10.1016/j.ijheatmasstransfer.2007.11.038>.
 33. Khan Masood, Khan Waqar Azeem. Steady flow of Burgers nanofluid over a stretching surface with heat generation/absorption. *J Braz Soc Mech Sci Eng.* 2016;38:2359–67. <https://doi.org/10.1007/s40430-014-0290-4>.
 34. Murthy PVS, RamReddy C, Chamkha AJ, Rashad AM. Significance of viscous dissipation and chemical reaction on convective transport in a boundary layer stagnation point flow past a stretching/shrinking sheet in a nanofluid. *J Nanoflu.* 2015;4(2):214–22. <https://doi.org/10.1166/jon.2015.1136>.
 35. Hussain SM, Jain J, Seth GS, Rashidi MM. Effect of Thermal Radiation on magneto-nanofluids free convective flow over an accelerated moving ramped temperature plate. *Sci Ira B.* 2018;25(3):1243–57. <https://doi.org/10.24200/SCI.2017.4333>.
 36. Nasir S, Islam S, Gul T, Khan ZS, Khan MA, Khan W, Khan S. Three-dimensional rotating flow of MHD single wall carbon nanotubes over a stretching sheet in presence of thermal radiation. *App Nanosci.* 2018;8(1):1361–78. <https://doi.org/10.1007/s13204-018-0766-0>.
 37. Dianchen Lu, Ramzan M, ul Huda N, Chung JD, Farooq U. Non-linear radiation effect on MHD carreau nanofluid flow over a radially stretching surface with zero mass flux at the surface. *Sci Rep.* 2018;8(1):1–17. <https://doi.org/10.1038/s41598-018-22000-w>.
 38. Mishra Ashish, Kumar Manoj. Thermal performance of MHD nanofluid flow over a stretching sheet due to viscous dissipation, Joule heating, and Thermal radiation. *Int J of App and Comp Math.* 2020;6(1):1–17. <https://doi.org/10.1007/s40819-020-00869-4>.
 39. Srinivasa Rao A, Dasaradha Ramaiah K, Kotha Gangadhar, Venkata Subba Rao M, Chamkha Ali J. A spectral relaxation approach for boundary layer flow of nanofluid past an exponentially stretching surface with variable suction in the presence of Heat Source/Sink with viscous dissipation. *Arab J for Sci Eng.* 2021;46(1):7509–20. <https://doi.org/10.1007/s13369-021-05422-z>.
 40. Imran Siddique, Sohaib Abdal, Irfan Saif Ud, Din JanAwrejcewicz, Pawowski Witold, Hussain Sajjad. Significance of concentration-dependent viscosity on the dynamics of tangent hyperbolic nanofluid subject to motile microorganisms over a non-linear stretching surface. *Sci Rep.* 2022;12(1):1–17. <https://doi.org/10.1038/s41598-022-16601-9>.
 41. Ramesh GK, Madhukesh JK, Khan Umair, Syed Hussain M, Ahmed Galal M. Inspection of hybrid nanoparticles flow across a nonlinear /linear stretching surface when heat sink/source and thermophoresis particle deposition impacts are significant. *Int J Mod Phy B.* 2023. <https://doi.org/10.1142/S021797922350008X>.
 42. Harish Babu D, Kumaraswamy Naidu K, Satya Deo, Satya Narayana PV. Impacts of inclined Lorentz forces on hybrid CNT's over an exponentially stretching sheet with slip flow. *Int J Mod Sim.* 2023;43(3):310–24. <https://doi.org/10.1080/02286203.2022.2079109>.
 43. Nayak MK, Dogonchi AS, Rahbari A. Free convection of Al₂O₃-water nanofluid inside a hexagonal-shaped enclosure with cold diamond-shaped obstacles and periodic magnetic field. *Cas Stu in Therm Engg.* 2023;50:103429. <https://doi.org/10.1016/j.csite.2023.103429>.
 44. Ghalambaz M, Grosan T, Pop I. Mixed convection boundary layer flow and heat transfer over a vertical plate embedded in a porous medium filled with a suspension of nano-encapsulated phase change materials. *Journal of Molecular Liquids.* 2019;293(1):1–9. <https://doi.org/10.1016/j.molliq.2019.111432>.
 45. Ghalambaz Mohammad, Jin Haichuan, Bagheri Amirhossein, Younis Obai, Wen Dongsheng. Convective flow and heat transfer of nano-encapsulated phase change material (NEPCM) dispersions along a vertical surface. *Fact Uni Ser Mech Engg.* 2022;20(3):519–38. <https://doi.org/10.22190/FUME220603034G>.
 46. Ghalambaz Mehdi, Mozaffari Masoud, Yazdani Shima, Abbaszadeh Mohammad, Sheremet Mikhail, Ghalambaz Mohammad. Conjugate entropy generation and heat transfer of a dilute suspension of nano-encapsulated phase change material in a partially heated wall cavity. *Rep in Mech Engg.* 2023;4(1):175–92. <https://doi.org/10.31181/rme040115092023g>.
 47. Magyari E, Pantokratoras A. Note on the effect of thermal radiation in the linearized Rosseland approximation on the heat transfer characteristics of various boundary layer flows. *Int Comm Heat Mass Trans.* 2011;38(5):554–6. <https://doi.org/10.1016/j.icheatmasstransfer.2011.03.006>.
 48. Waini I, Ishak A, Pop I. Multiple solutions of the unsteady hybrid nanofluid flow over a rotating disk with stability analysis. *Eur J Mech - B/Flu.* 2022;94:121–7. <https://doi.org/10.1016/j.euromechflu.2022.02.011>.
 49. Eid MR, Nafe MA. Thermal conductivity variation and heat generation effects on magneto-hybrid nanofluid flow in a porous medium with slip condition. *Wav Ran Comp Med.* 2022;32(1):1103–27. <https://doi.org/10.1080/17455030.2020.1810365>.
 50. Aziz A, Jamshed W, Aziz T. Mathematical Model for Thermal and Entropy Analysis of Thermal Solar Collectors by Using Maxwell Nanofluids with Slip Conditions. *Therm Rad Variable Therm*

- Conduct, *Open Phy.* 2018;16(1):123–36. <https://doi.org/10.1515/phys-2018-0020>.
51. Hamid M, Usman M, Zubair T, Haq RU, Wanga W. Shape effects of MoS₂ nanoparticles on rotating flow of nanofluid along a stretching surface with variable thermal conductivity: A Galerkin approach. *Int J Heat Mass Trans.* 2018;124(1):706–14. <https://doi.org/10.1016/j.ijheatmasstransfer.2018.03.108>.
 52. Usman M, Hamid M, Zubair T, Haq RU, Wang W. Cu/AIO/water hybrid nanofluid through a permeable surface in the presence of nonlinear radiation and variable thermal conductivity via LSM. *Int J of Heat and Mass Trans.* 2018;126(1):1347–56.
 53. Abu Hamdeh NH, Aljinaidi AA, Eltaher MA, Almitani KH, Alnefaie KA, Abusorrah AM, Safaei MR. Implicit finite difference simulation of Prandtl-Eyring nanofluid over a flat plate with variable thermal conductivity: A Tiwari and das model. *Math.* 2021;9(24):3153. <https://doi.org/10.3390/math9243153>.
 54. Pal D, Mandal G. Magneto-hydrodynamic nonlinear thermal radiative heat transfer of nanofluids over a flat plate in a porous medium in existence of variable thermal conductivity and chemical reaction. *Int J of Amb Ene.* 2019;42(10):1167–77. <https://doi.org/10.1080/01430750.2019.1592776>.
 55. Weidman PD, Kubitschek DG, Davis AMJ. The effect of transpiration on self-similar boundary layer flow over moving surface. *Int J Eng Sci.* 2006;44(11–12):730–7. <https://doi.org/10.1016/j.ijengsci.2006.04.005>.
 56. Harris SD, Ingham DB, Pop I. Mixed convection boundary layer flow near the stagnation point on a vertical surface in a porous medium: Brinkman model with slip. *Trans Por Med.* 2009;77(1):267–85. <https://doi.org/10.1007/s11242-008-9309-6>.
 57. Abd El-Aziz M. Viscous dissipation effect on mixed convection flow of a micropolar fluid over an exponentially stretching sheet. *Can J Phys.* 2009;87(4):359–68. <https://doi.org/10.1139/P09-047>.
 58. Ishak A. MHD boundary layer flow due to exponentially stretching sheet with radiation effect. *Sns Mal.* 2011;40(1):391–5.
 59. Wahid NS, Arifin NM, Khashiie NS, Pop I. Hybrid nanofluid slip flow over an exponentially stretching/shrinking permeable sheet with heat generation. *Mathematics.* 2020;9(1):1–20. <https://doi.org/10.3390/math9010030>.
 60. Waini Iskandar, Ishak Anuar, Pop Ioan. Hybrid nano fluid flow induced by an exponentially shrinking sheet. *Chi J Phy.* 2020;68(1):468–82. <https://doi.org/10.1016/j.cjph.2019.12.015>.
 61. Ghosh S, Mukhopadhyay S. Stability analysis for model based study of nanofluid flow over an exponentially shrinking permeable sheet in presence of slip. *Neu Comp App.* 2020;32:7201–11. <https://doi.org/10.1007/s00521-019-04221-w>.
 62. Mints HA, Roy G, Nguyen CT, Doucet D. New temperature dependent thermal conductivity data for water-based nanofluids. *Int J Ther Sci.* 2009;48(2):363–71. <https://doi.org/10.1016/j.ijthermalsci.2008.03.009>.
 63. Merkin JH. Mixed convection boundary layer flow on a vertical surface in a saturated porous medium. *J Eng Math.* 1980;14:301–13. <https://doi.org/10.1007/BF00052913>.

Publisher's Note Springer Nature remains neutral with regard to jurisdictional claims in published maps and institutional affiliations.

Springer Nature or its licensor (e.g. a society or other partner) holds exclusive rights to this article under a publishing agreement with the author(s) or other rightsholder(s); author self-archiving of the accepted manuscript version of this article is solely governed by the terms of such publishing agreement and applicable law.